Exp Fluids (2015) 56:174
DOI 10.1007/s00348-015-2045-0

RESEARCH ARTICLE

# A detailed procedure for measuring turbulent velocity fluctuations using constant-voltage anemometry

**Abdelouahab Mohammed-Taifour[1] · Julien Weiss[1] · Atabak Sadeghi[2] · Jérôme Vétel[2] · Emmanuel Jondeau[3] · Geneviève Comte-Bellot[3]**

Received: 12 May 2015 / Revised: 14 August 2015 / Accepted: 17 August 2015 / Published online: 28 August 2015


**Abstract** A detailed procedure to use a constant-voltage anemometer (CVA) for the accurate measurement of turbulent flows is proposed. The procedure is based on the usual small-perturbation analysis of hot-wire signals. It consists in three steps: (1) the calibration of internal elements, required to estimate the two main electrical parameters of the CVA circuitry that are needed in the data analysis, (2) a flow calibration to relate the CVA output voltage and the hot-wire time constant to the flow velocity, and (3) a data-processing algorithm to recover the fluctuating flow quantities from the output voltage. The procedure is tested in two classical turbulent flows: a zero-pressure-gradient boundary layer and a round jet. In both cases, the CVA results are shown to be essentially indistinguishable from the results obtained with a research-grade constant-temperature anemometer.

## 1 Introduction

The constant-voltage hot-wire anemometer (CVA) has now been in use for more than 20 years (Mangalam et al. 1992). Its function principle was described in detail by Sarma (1998), and its performance was compared with the more common constant-temperature anemometer (CTA) by Comte-Bellot et al. (1999), Kegerise and Spina (2000a, b) and Weiss et al. (2005). The CVA circuit was analyzed in terms of signal-to-noise ratio by Weiss and Comte-Bellot (2004) and in terms of cable-resistance effects by Comte-Bellot et al. (2004). The CVA was used in experiments with fluid temperature drifts, either in a standard laboratory setting (Truzzi et al. 2002) or within an automated procedure (Sarma and Lankes 1999; Sarma and Comte-Bellot 2002). More recently, the CVA was also shown to be advantageous for the elimination of nonlinear effects in the presence of large velocity and temperature fluctuations (Berson et al. 2009, 2010).

Over the years, the main advantage of the CVA was found to be its wider frequency bandwidth compared to the CTA. For example, Weiss et al. (2005) observed a cutoff frequency of more than 450 kHz for a CVA operated with a typical 5-μm hot-wire probe at a Mach number of 2.5, whereas the cutoff frequency of a research-grade CTA in the same conditions was only about 100 kHz. The CVA circuit also exhibits a well-behaved second-order system behavior close to its cutoff frequency (Sarma 1998), whereas the CTA's frequency response strongly depends on its tuning parameters (Weiss et al. 2001, 2013). Indeed, Hutchins et al. (2015) recently demonstrated that the under- or over-damped characteristics of CTA systems near their cutoff frequency can lead to significant errors on the measurement of turbulent spectra in high-Reynolds-number, wall-bounded flows. The favorable characteristics of the CVA in terms of frequency response thus make it particularly attractive for measurements where the frequency content of the turbulent fluctuations is large, for example in high-speed or high-Reynolds-number turbulent flows.

Most of the existing articles on the topic tend to analyze specific aspects of the CVA operation. In contrast,

✉ Julien Weiss
julien.weiss@etsmtl.ca

1 Laboratoire TFT, École de Technologie Supérieure, 1100 Notre-Dame Ouest, Montréal, QC H3C 1K3, Canada

2 LADYF, Polytechnique Montréal, C.P. 6079, Succursale Centre-Ville, Montréal, QC H3C 3A7, Canada

3 LMFA, UMR CNRS 5509, École Centrale de Lyon, C.P. 6079, 36 Avenue Guy de Collongue, 69134 Ecully Cedex, France

the purpose of the present article is to establish a practical, robust methodology for turbulence measurements with a CVA. While especially targeted to subsonic applications, the proposed methodology can also be applied to high-speed compressible flows, provided that the hot-wire calibration law is modified accordingly (Comte-Bellot 2007). The article is organized as follows. Section 2 summarizes the function principle of the CVA and highlights its key differences compared to the more classical CTA. Section 3 then describes the proposed experimental procedure. Finally, Sect. 4 illustrates the use of the proposed methodology by comparing CVA and CTA measurements performed in a turbulent boundary layer and in a subsonic jet.

## 2 Function principle of the CVA

Figure 1 shows a schematic diagram of the CVA circuit. The circuit maintains the voltage $V_w$ across the hot-wire of resistance $R_w$ and its connecting cable $r_L$ constant. The resistance $r_L$ takes into account the total resistance of the connecting cable, that is, the cable itself, the probe support, the hot-wire "prongs," and any connector present between the sensor and the electronic circuit (Comte-Bellot et al. 2004). Resistors $R_{2a}$ and $R_{2b}$, together with capacitor $C$, act as a high-pass amplifier to compensate for the hot-wire thermal inertia. The circuit presented in Fig. 1 is a typical non-inverting amplifier configuration (Horowitz and Hill 1989). Earlier versions of the CVA used an inverting configuration that essentially achieves the same objective of maintaining $V_w$ constant across the hot-wire. Detailed analysis of this earlier system were presented by Sarma (1998), Comte-Bellot et al. (2004) and Berson et al. (2009). The main difference between the inverting and non-inverting configurations is the presence of another resistor (called $R_F$ in earlier publications) that does not appear in the non-inverting configuration.

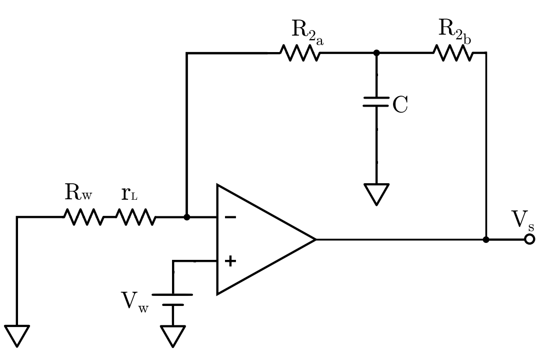


**Fig. 1** Schematic diagram of the CVA circuit. $R_w$ stands for the hot-wire resistance and $r_L$ for the resistance of its connecting cable

With the notations of Fig. 1, the output voltage $V_s$ is given by:

$$V_s = V_w\left(1 + \frac{R_2}{R_w + r_L}\right) - T_C\frac{R_2 V_w}{(R_w + r_L)^2}\frac{\mathrm{d}R_w}{\mathrm{d}t}, \tag{1}$$

where $R_2 = R_{2a} + R_{2b}$. The time constant $T_C = R_{2a}R_{2b}C/R_2$ is the hardware compensation setting of the circuit. Equation 1 is valid up to the circuit's cutoff frequency, which mainly depends on the operational amplifier's characteristics. The reader is referred to Sarma (1998) for more details about the frequency response of the CVA and its actual measurement. In current CVA units, the cut-off frequency is of the order of 450 kHz.

In standard experimental situations, the fluctuation level is assumed sufficiently small to invoke the "small-perturbation hypothesis" and all equations are linearized (Bailly and Comte-Bellot 2015). Equation 1 then becomes:

$$v_s' = -\frac{R_2 V_w}{\left(\overline{R}_w + r_L\right)^2}\left(r_w' + T_C\frac{\mathrm{d}r_w'}{\mathrm{d}t}\right), \tag{2}$$

which relates a small fluctuation of output voltage $v_s'(t)$ to a small fluctuation $r_w'(t)$ in wire resistance. In Eq. 2, $\overline{R}_w$ is the mean value of the wire resistance around which the fluctuations appear. The minus sign on the right-hand side of Eq. 2 reminds us that a decrease in $R_w$ (i.e., a cooling of the hot-wire generated through an increase in velocity, for example) results in an increase in $V_s$, in accordance with Eq. 1.

The fluctuation $r_w'(t)$ of the wire resistance is related to a fluctuation $u'(t)$ in the flow velocity or to a fluctuation $\theta_a'(t)$ in the ambient fluid temperature according to the usual first-order approximation of a hot-wire filament:

$$r_w' + M_{\mathrm{CVA}}\frac{\mathrm{d}r_w'}{\mathrm{d}t} = S_U u' + S_{T_a}\theta_a', \tag{3}$$

where $M_{\mathrm{CVA}}$ is the hot-wire time constant in the CVA operation mode, $S_U$ the wire sensitivity to the flow velocity, and $S_{T_a}$ its sensitivity to the mean fluid temperature $T_a$. Both sensitivities relate to a wire operated at constant voltage and semiempirical estimates of $S_U$ and $S_{T_a}$ are available in Comte-Bellot (2007).

Following Bailly and Comte-Bellot (2015), we now introduce an ideal hot-wire without any thermal lag. Its electrical resistance $R_w^*$ is denoted with a star to indicate an ideal wire quantity. When connected to a CVA circuit, the output voltage $V_s^*$ that would be measured with this ideal wire reads:

$$V_s^* = V_w\left(1 + \frac{R_2}{R_w^* + r_L}\right), \tag{4}$$

since no hardware compensation is necessary for the ideal wire (i.e., $T_C = 0$). Linearizing Eq. 4 using $\overline{R_w^*} = \overline{R}_w$ and

$\overline{V_s^*} = \overline{V}_s$ leads to an expression for the ideal fluctuating voltage $v_s'^*$:

$$v_s'^* = -\frac{R_2 V_w}{(\overline{R}_w + r_L)^2} r_w'^*, \tag{5}$$

where the fluctuating resistance $r_w'^*$ of the ideal wire is related to that of the real wire $r_w'$ and the fluctuations in the flow by:

$$r_w'^* = r_w' + M_{\mathrm{CVA}} \frac{\mathrm{d}r_w'}{\mathrm{d}t} = S_U u' + S_{T_a} \theta_a'. \tag{6}$$

Combining the first equality in Eq. 6 with Eq. 2, we obtain:

$$v_s' = -\frac{R_2 V_w}{\left(\overline{R}_w + r_L\right)^2} \left( r_w'^* + (T_{\mathrm{C}} - M_{\mathrm{CVA}}) \frac{\mathrm{d}r_w'}{\mathrm{d}t} \right). \tag{7}$$

Comparing Eq. 5 with Eq. 7 demonstrates that the ideal fluctuating output voltage $v_s'^*$ can be recovered from measurements obtained with a real hot-wire when $T_{\mathrm{C}}$ exactly matches $M_{\mathrm{CVA}}$. Furthermore, in this case the fluctuating CVA, output voltage will follow the flow fluctuations without any time lag.

In practice, since $M_{\mathrm{CVA}}$ depends on the mean flow quantities, $T_{\mathrm{C}}$ rarely matches $M_{\mathrm{CVA}}$ and a software correction is required to correct for the mismatch (Sarma et al. 1998). This requires an accurate determination of both $T_{\mathrm{C}}$ and $M_{\mathrm{CVA}}$. The software correction consists in defining a corrected output voltage that takes into account the difference between the partial hardware correction from the CVA circuit ($T_{\mathrm{C}}$) and the hot-wire time constant ($M_{\mathrm{CVA}}$). This means that the corrected output voltage corresponds to the case of a CVA circuit operated with an ideal wire, even when $T_{\mathrm{C}} \neq M_{\mathrm{CVA}}$.

In the frequency domain, using the same notations as above, the correction is defined by:

$$v_s'^*(s) = v_s'(s) \left[ \frac{1 + M_{\mathrm{CVA}} s}{1 + T_{\mathrm{C}} s} \right], \tag{8}$$

where $s$ is the Laplace variable. To see why the right-hand side of Eq. 8 corresponds to the case of an ideal wire, Eqs. 2 and 3 can be transformed in the frequency domain and combined to give:

$$v_s'(s) = -\frac{R_2 V_w}{\left(\overline{R}_w + r_L\right)^2} \left[ \frac{1 + T_{\mathrm{C}} s}{1 + M_{\mathrm{CVA}} s} \right] \left[ S_U u'(s) + S_{T_a} \theta_a'(s) \right]. \tag{9}$$

Introducing the software-corrected output voltage $v_s'^*(s)$ from Eq. 8 leads to:

$$\begin{aligned} v_s'^*(s) &= -\frac{R_2 V_w}{\left(\overline{R}_w + r_L\right)^2} \left[ S_U u'(s) + S_{T_a} \theta_a'(s) \right] \\ &= -\frac{R_2 V_w}{\left(\overline{R}_w + r_L\right)^2} r_w'^*(s). \end{aligned} \tag{10}$$

Finally, comparing Eq. 10 with its time-domain equivalent Eq. 5 proves that the software-corrected output voltage is indeed equal to the fluctuating voltage of an ideal, thermal-lag-free, hot-wire.

Equations 1 and 7 illustrate the two main differences of the CVA anemometer compared to the CTA anemometer. First, the average hot-wire resistance $\overline{R}_w$, and hence its temperature $\overline{T}_w$ is free to change with a variation of mean flow quantities. This is in direct contrast to the CTA, where $\overline{R}_w$ is maintained constant by the feedback circuit. Second, from a control perspective, the compensation for thermal inertia occurs in series with the output, and not within the feedback system. This means that the user keeps the responsibility of the compensation, contrary to the CTA where the compensation is automatically performed by the feedback circuit and thus transparent to the user (assuming a correct tuning of the dynamic parameters to obtain a satisfactory frequency response). This also means that accurate values of $T_{\mathrm{C}}$ and $M_{\mathrm{CVA}}$ need to be determined in addition to the CVA output voltage $V_s$ in order to implement Eq. 8. Finally, we emphasize that the present treatment is restricted to flow fluctuations of relatively low amplitude, in which case the equations can be linearized. The case of large-amplitude fluctuations is treated in detail by Berson et al. (2009, 2010).

## 3 Proposed experimental procedure

The proposed experimental procedure consists in three steps. First, the calibration of internal electronic elements, which is performed only once, and whose purpose is to determine the electronic parameters $R_2$ and $T_{\mathrm{C}}$ that are relevant for subsequent data processing. Second, a flow calibration, which consists in relating the average CVA output voltage $\overline{V}_s$ and the hot-wire time constant $M_{\mathrm{CVA}}$ to average flow parameters. Finally, a measurement of the time trace $V_s(t)$ in the turbulent flow of interest with subsequent data processing to recover the true velocity trace $U(t)$.

### 3.1 Calibration of internal elements

As explained in Sect. 2, in a CVA the average hot-wire resistance $\overline{R}_w$ depends on the average flow parameters. It is necessary to determine $\overline{R}_w$'s numerical value in order to estimate the wire overheat and to perform the flow calibration (see Sect. 3.2). The average wire resistance can be obtained by time-averaging Eq. 1:

$$\overline{V}_s = V_w \left( 1 + \frac{R_2}{\overline{R}_w + r_L} \right). \tag{11}$$

In Eq. 11, the unknown is $\overline{R}_w$ and the signal to be acquired is $\overline{V}_s \cdot r_L$ is a constant that can be measured prior to an

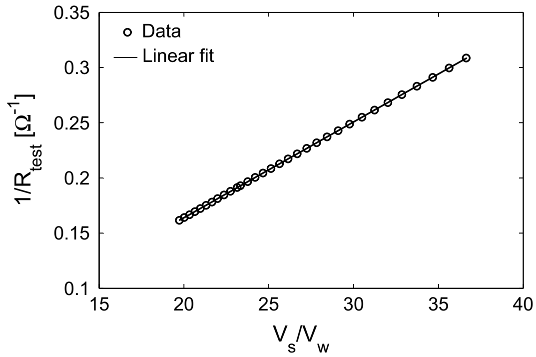


**Fig. 2** Electrical test to obtain $R_2$ (see Eq. 12)

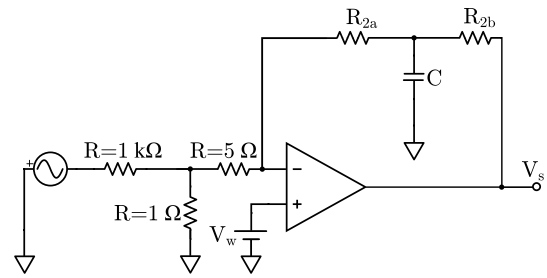


**Fig. 3** Sine-wave test setup for $T_C$ determination

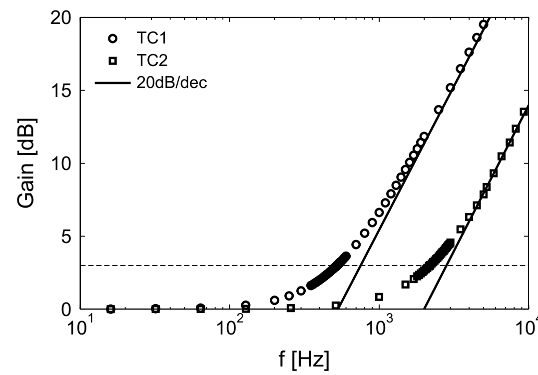


**Fig. 4** Sine-wave test results: 3 dB line at 519 Hz for $T_{C_1}$ and 2175 Hz for $T_{C_2}$

experiment and $V_w$ is a control parameter that is maintained constant by the circuit. Typically, a value of $V_w = 0.5$ V is convenient for a 5-µm wire in subsonic flows. $R_2$ is an electrical parameter that is constant for each CVA unit. Its value is required to solve for $\overline{R}_w$ from the measurement of $\overline{V}_s$.

The value of $R_2$ can be obtained by a simple electrical test consisting in connecting a series of precision resistors $R_{\text{test}}$ in place of the hot-wire and recording the output voltage $V_s$ when the wire voltage $V_w$ is held constant. When $R_{\text{test}}$ is used instead of $R_w + r_L$, Eq. 11 is equivalent to:

$$\frac{1}{R_{\text{test}}} = \frac{1}{R_2}\left(\frac{V_s}{V_w} - 1\right). \tag{12}$$

Thus, by plotting $1/R_{\text{test}}$ as a function of $V_s/V_w$, a straight line of slope $1/R_2$ is obtained.

Figure 2 shows an example of diagram obtained by this procedure on a Tao Systems Model 4-600 CVA unit. A series of precision resistors ranging from $R_{\text{test}} = 3\ \Omega$ to $R_{\text{test}} = 6\ \Omega$ (i.e., typical values of the hot-wire resistance) was used to generate the plot, while $V_w$ was maintained constant at $V_w = 0.5$ V. From the slope of the straight line we obtain $R_2 = 115\ \Omega$. This value is then stored in the data-processing algorithm and enable the computation of $\overline{R}_w$ from the measurement of $\overline{V}_s$ and the use of Eq. 11.

In addition to $R_2$, the exact value of $T_C$ is required for the software correction procedure defined by Eq. 8. $T_C$ can be determined by an electrical "sine-wave test," as originally proposed by Sarma (1998) for the measurement of the CVA frequency response. The circuit described in Fig. 3 is used to inject a fluctuating voltage in the hardware compensation circuit. In this experiment, the hot-wire is not connected to the circuit but is replaced by two fixed resistors of 1 and 5 Ω, respectively.

As an example, a sinusoidal voltage of 0.3 V amplitude and varying frequency was injected into the Model 4-600 CVA unit. This unit features two settings for the hardware compensation: $T_{C_1}$ and $T_{C_2}$. The resulting Bode plots for both settings are presented in Fig. 4. As expected, the system behaves as a first-order, high-pass amplifier with 3 dB cutoff values of $T_{C_1} = 306\,\mu$s (519 Hz) and $T_{C_2} = 73\,\mu$s (2175 Hz), respectively. Repeated experiments on different dates have demonstrated a standard deviation of approximately 0.5 % in the values of $T_C$ obtained by this method (Sadeghi 2014).

To demonstrate the effectiveness of the procedure, the fluctuating output voltage of the same CVA unit was acquired in the shear layer bordering a turbulent jet (see Sect. 4.2). Three settings of $T_C$ were used for this experiments: $T_C = T_{C_1}, T_C = T_{C_2}$, and $T_C = 0$. The power spectral density (PSD) of the signals measured with $T_{C_1}$ and $T_{C_2}$ were then reverse-corrected to a value of $T_C = 0$ using the $T_C$ values obtained from the sine-wave test ($T_{C_1} = 306\,\mu$s and $T_{C_2} = 73\,\mu$s). If those values are correct, then the three PSDs should overlap. Figure 5 shows that this is indeed the case: the black curve was obtained from the $T_C = 0$ signal, while the red and blue curves correspond to the reverse-corrected PSDs obtained with the $T_{C_1}$ and $T_{C_2}$ settings, respectively. All three curves are superimposed in a wide range of frequencies, which validates the results of the sine-wave test. Note also that the constant PSD levels reached at high frequencies represent the manifestation of electronic noise. A lower noise floor is obtained when a time constant $T_C$ is

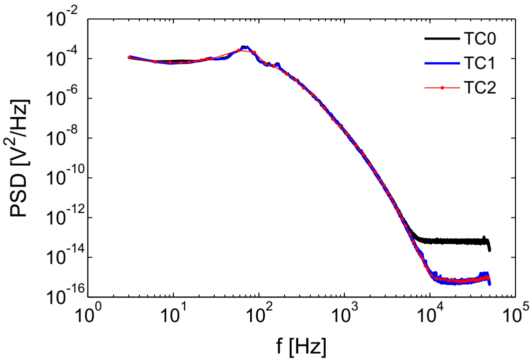


**Fig. 5** PSD of output voltages measured with $T_C = 0, T_{C_1}$ (reverse-corrected to a value of $T_C = 0$) and $T_{C_2}$ (reverse-corrected to a value of $T_C = 0$)

operated, which illustrates the benefit of using an analog amplification circuit in a hot-wire anemometer.

### 3.2 Flow calibration

Calibration of any type of hot-wire anemometer is required in order to relate its output voltage to the flow velocity. In the case of the CVA, a calibration is also required to obtain the value of $M_{\mathrm{CVA}}$, which is needed for the software correction procedure (Eq. 8).

#### *3.2.1 Velocity calibration*

Different calibration laws have been proposed over the years to relate the output voltage of hot-wire anemometers to the flow velocity. Most of them are based on a modified version of King's law (Bruun 1995), whereas others are based on more general polynomial laws (Perry 1982). The general idea is to use a semiempirical relationship for the convective heat transfer generated by the air flow, and to balance it with the Joule heating of the hot-wire. In this work we use the heat transfer law by Collis and Williams (1959), which is an improvement in the basic King's law.

The general formulation of Collis and Williams' heat transfer law reads:

$$\left(\frac{T_f}{T_a}\right)^{-0.17} Nu_w = A_1 + B_1 Re_w^n, \tag{13}$$

where $T_f$ is the "film temperature" defined as $T_f = (T_w + T_a)/2$, i.e., the average of the wire temperature $T_w$ and the fluid temperature $T_a$; $Nu_w$ and $Re_w$ are the Nusselt and Reynolds numbers of the cylindrical hot-wire, and $A_1, B_1$, and $n$ are constants. In Eq. 13, all flow parameters are evaluated at the film temperature $T_f$. Balancing the Joule heating and the convective heat transfer of the wire leads to the definition of a calibration constant CAL that can be written in terms of measurable quantities:

$$\mathrm{CAL} = \left(\frac{T_f}{T_a}\right)^{-0.17} \left(\frac{V_w^2}{R_w^*(R_w^* - R_a)}\right) = A + BU^n. \tag{14}$$

In Eq. 14, all quantities are supposed to be independent of time as they are acquired in a dedicated calibration facility (free stream of a wind tunnel or potential core of a jet). Therefore, $R_w^* = \overline{R}_w$ since there is no need to compensate for the wire thermal inertia. This also means that $R_w^*$ can directly be obtained from the measurement of $\overline{V}_s$ and the use of Eq. 11. In Eq. 14 $R_a$ is the wire resistance at the temperature $T_a$ of the air. $R_a$ is generally obtained by measuring the air temperature with a dedicated sensor and by assuming a linear relationship between temperature and resistance, so that $R_a = R_0(1 + \chi_0(T_a - T_0))$, where $R_0$ is the wire resistance at a reference temperature $T_0$ and $\chi_0$ is the temperature coefficient of resistance (typically, $\chi_0 \simeq 0.004\,K^{-1}$ for tungsten wires). Alternatively, $R_a$ can also be obtained directly with the CVA circuit by quickly changing the wire voltage $V_w$, as proposed by Sarma and Comte-Bellot (2002). Note also that $A = A_1 \frac{\pi l_w \lambda_f}{R_0 \chi_0}$ and $B = B_1 \frac{\pi l_w \lambda_f}{R_0 \chi_0} \left(\frac{\rho_f d_w}{\mu_f}\right)^n$, where $\lambda_f$, $\rho_f$, and $\mu_f$ are the thermal conductivity, density, and dynamic viscosity of the air at the film temperature $T_f$, and where $d_w$ and $l_w$ are the diameter and length of the wire, respectively.

The main advantage of using the CAL variable is that it takes into account any change of ambient temperature during an experiment since $T_a$ enters its definition. Thus, once $T_a$ is measured independently with a temperature sensor, the use of CAL automatically corrects for any temperature drift.

The calibration constants $A$ and $B$ can be obtained from a linear regression of CAL as a function of $U^n$. The best value of $n$ is chosen so as to minimize the residual least-squares error. Typically, a value close to $n \simeq 0.5$ is obtained. Figure 6 shows examples of calibration curves obtained in the potential flow of a low-speed wind tunnel. The same hot-wire ($d_w \simeq 5\,\mu$m and $l_w \simeq 1.2$ mm) was calibrated sequentially with a Tao Systems Model 4-600 CVA unit and a DISA 55M10 CTA unit. It is obvious that the calibration curves are almost identical, which is expected given that the CAL variable is only dependent on wire and fluid parameters. The small residual difference might be caused by a small uncertainty in $R_w$ for the CTA circuit. Indeed, for the case of the CTA, $R_w$ is typically estimated by assuming that the Wheatstone bridge is exactly balanced, which is not completely accurate (Weiss 2003).

#### *3.2.2 $M_{CVA}$ calibration*

The software correction defined by Eq. 8 requires the measurement of the wire time constant $M_{\mathrm{CVA}}$. It is obtained

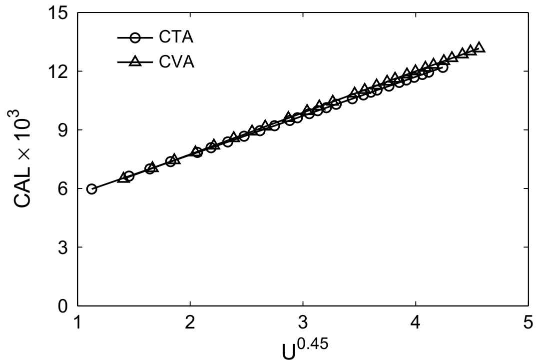


**Fig. 6** Example of velocity calibration curves for CVA and CTA operation. The correlation coefficient of the linear least square fit obtained for the CVA and the CTA is 0.99989 and 0.99987, respectively

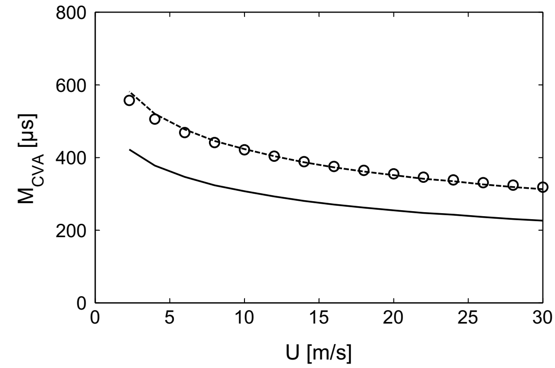


**Fig. 8** $M_{\rm CVA}$ values at different velocities, $V_w = 0.5$ V. *Circles* experimental values, *dashed line* Eq. 15 with $m_w c_w/\chi_0 R_0$ selected to fit the experimental data, *solid line* Eq. 15 with $m_w c_w/\chi_0 R_0$ computed from the nominal wire dimensions and material properties

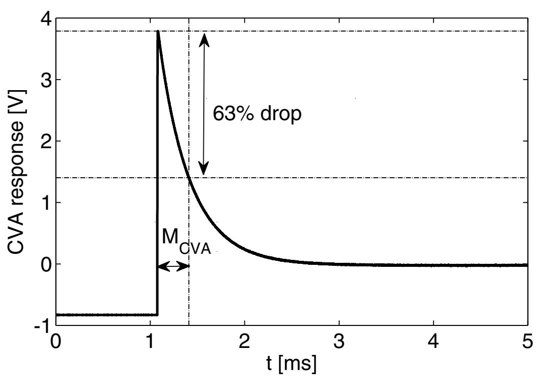


**Fig. 7** Electrical square-wave test to compute $M_{\rm CVA}$

by using the dedicated time constant measurement (TCM) module of the CVA circuit. As illustrated in Sarma (1998), the TCM module consists in an uncompensated ($T_{\rm C} = 0$) CVA channel that injects an electrical square-wave signal into the wire. The value of $M_{\rm CVA}$ is obtained by processing the resulting output voltage.

Figure 7 shows an example of signal obtained by connecting an Auspex Scientific, 5-µm hot-wire to the TCM module of the Model 4-600 CVA unit at a velocity of 25 m/s in the potential flow of a wind tunnel (see Sect. 4.1). The signal shows a rising edge followed by an exponential decay, in accordance with the first-order model typically assumed for cylindrical hot-wire filaments (Bailly and Comte-Bellot 2015). The TCM module is designed so that the exponential decay asymptotes toward 0 V. As described in Fig. 7, the value of $M_{\rm CVA}$ is readily obtained by the distance between the signal's maximum and the position where it reaches 63 % of decay. Note that a sufficient sampling rate is required in order to digitally resolve the signal's maximum: the data shown in Fig. 7 were obtained with a sampling rate of 1 MHz, which will probably be sufficient for most applications. In some cases, phase-averaging of several square-wave periods might be required in order to smooth out fluctuations of the output voltage.

A semiempirical expression of $M_{\rm CVA}$, including the effect of the lead cable, was derived by Comte-Bellot et al. (2004). It reads:

$$M_{\rm CVA} = \frac{1}{V_w^2}\frac{m_w c_w}{\chi_0 R_0}(\overline{R}_w + r_L)^2 \frac{a_w}{1+2a_w} \times LM, \tag{15}$$

where $a_w = (\overline{R}_w - R_a)/\overline{R}_w$ is the wire overheat ratio, $m_w$ and $c_w$ are, respectively, the mass and the specific heat of the wire, and where $LM$ is a correction factor that comes from the connecting cable:

$$LM = \left[1 + \frac{r_L}{R_a(1+a_w)}\right]\left[1 + \frac{r_L}{R_a(1+a_w)(1+2a_w)}\right]^{-1}. \tag{16}$$

Equation 15 shows that $M_{\rm CVA}$ depends on the wire overheat ratio $a_w$, which itself depends on the mean flow velocity when $V_w$ is maintained constant. Thus, for a series of measurements where the mean velocity varies (e.g., at different positions in a stationary turbulent flow), a different value of $M_{\rm CVA}$ needs to be used at each position. The recommended procedure is to measure $M_{\rm CVA}$ for different values of $U$ in parallel with the velocity calibration. This is presented in Fig. 8, which shows the value of $M_{\rm CVA}$, obtained using the procedure illustrated in Fig. 7, for different velocities in the potential flow of a wind tunnel. The wire voltage was maintained constant at $V_w = 0.5$ V for these measurements. It can be seen that $M_{\rm CVA}$ decreases from about 560 µs at $U \simeq 2$ m/s to about 320 µs at $U = 30$ m/s. Also shown in the figure are the values obtained by using Eq. 15. The dashed line was obtained by using an average value of $m_w c_w/\chi_0 R_0 = 8 \times 10^{-6}$ A$^2$ selected to fit the experimental data, whereas the solid line was computed from the nominal wire properties (tungsten wire, $d_w \simeq 5$µm, and $l_w \simeq 1.2$

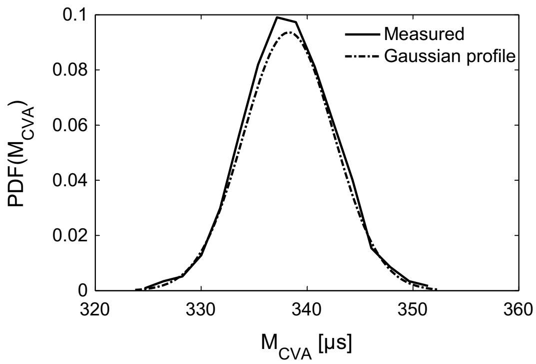


**Fig. 9** Probability density function of $M_{\mathrm{CVA}}$ measurements (700 square-wave samples taken at 25 m/s). Mean value: $\mu_{M_{\mathrm{CVA}}} = 338\,\mu\mathrm{s}$, standard deviation: $\sigma_{M_{\mathrm{CVA}}} = 4.3\,\mu\mathrm{s}$

mm). It is clear that the functional relationship described by Eq. 15 accurately models the experimental data. The nominal wire dimensions, however, are not accurate enough to enable a good estimation of $M_{\mathrm{CVA}}$. In practice, $M_{\mathrm{CVA}}$ can be obtained for any velocity by either interpolating through the experimental data points in Fig. 8, or using Eq. 15 with the value of $m_w c_w/\chi_0 R_0$ obtained experimentally with a few data points.

The variability in the measurement of $M_{\mathrm{CVA}}$ was investigated by recording 700 square-wave responses at a constant velocity of 25 m/s and automating the calculation of $M_{\mathrm{CVA}}$. Figure 9 shows an estimate of the probability density function of the measured values, which demonstrates a standard deviation of about 1.3 % in the potential flow of the wind tunnel. This value will be used in a later section to estimate the uncertainty associated with the time constant compensation procedure.

### 3.3 Turbulence measurements

Once all the steps above have been performed, the CVA can be used for turbulence measurements. This is done by selecting the same value of $V_w$ that was chosen during calibration and measuring a time trace of the output voltage $V_s(t)$. To convert $V_s(t)$ into $U(t)$, the output voltage is first split between its average value $\overline{V}_s$ and its fluctuating part $v'_s(t)$. Then, the software correction (Eq. 8) is applied to recover the fluctuating voltage of an ideal wire $v'^*_s(t)$. Adding the ideal fluctuating voltage $v'^*_s(t)$ to the average voltage $\overline{V}_s = \overline{V^*_s}$ then gives the time trace of the ideal, thermal-lag-free, output voltage $V^*_s(t)$, from which the ideal resistance $R^*_w(t)$ can be obtained using Eq. 4. In a final step, $R^*_w(t)$ is injected into Eq. 14 to recover $U(t)$. As mentioned above, this procedure automatically compensates for temperature drifts between calibration and experiments.

The software correction (Eq. 8) can either be implemented in the frequency or in the temporal domain. In the frequency domain, one can make use of the Fast Fourier Transform algorithm by replacing the Laplace variable $s$ by $2\pi jf$, where $f$ is the frequency and $j$ is the imaginary unit. Alternatively, one can use a discretization scheme to solve the temporal equivalent of Eq. 8 in the time domain. For example, Bailly and Comte-Bellot (2015) propose the following simple backward differencing scheme in terms of the $i$th and $(i-1)$th samples acquired at a sampling frequency $f_s$:

$$v'^*_s(i) = \frac{v'_s(i) + M_{\mathrm{CVA}} f_s \left[v'_s(i) - v'_s(i-1)\right] + T_C f_s v'^*_s(i-1)}{1 + T_C f_s} \tag{17}$$

## 4 Comparative measurements with CVA and CTA

The procedure described in this article was validated by performing turbulence measurements in two typical low-speed flows: a zero-pressure-gradient (ZPG) turbulent boundary layer and a turbulent jet. CVA measurements were performed with the Tao Systems Model 4-600 CVA unit described above and then compared to results obtained with a DISA 55M10 CTA unit. In each flow, the two anemometers were operated sequentially with the same hot-wire. The flow calibrations were respectively performed in the potential flow above the boundary layer and in the potential core of the jet. For both anemometers, the CAL variable described by Eq. 14 was used to convert the output voltage to velocity. The cutoff frequency of the CTA was adjusted to about 70 kHz in the free stream of the wind tunnel using an electrical square-wave test. The actual frequency response was then verified using the method of Weiss et al. (2001), which uses the normalized Fourier transform of the square-wave response to compute the CTA frequency response. The experiments reported in the present article were all performed with hot-wire filaments of 5 μm diameter. It is worth mentioning that Berson et al. (2010) successfully used a smaller wire of 2.5 μm nominal diameter, thereby demonstrating the usefulness of the CVA with small-diameter wires.

### 4.1 Turbulent boundary layer

Measurements were performed in the test-section of the TFT Boundary-Layer Wind Tunnel at École de technologie supérieure (Mohammed-Taifour et al. 2015). A boundary-layer profile was measured on the test-section centerline at a streamwise position 1.10 m downstream of the test-section entrance, in a region of zero pressure gradient. The wind tunnel reference velocity was $U_{\mathrm{ref}} = 25$ m/s, which resulted in a momentum thickness Reynolds number of $Re_\theta \simeq 5000$. At these flow conditions the 99 % boundary-layer thickness is $\delta_{99} = 27.8$ mm, the momentum thickness is $\theta = 3.0$ mm, the wall-friction coefficient is

$c_f = 3.1 \times 10^{-3}$, and the friction velocity is $u_\tau = 0.98$ m/s (Mohammed-Taifour et al. 2015).

An Auspex Scientific, single-normal hot-wire probe was traversed vertically using an automated positioning system having a relative accuracy of 0.5 µm. The wire voltage was held constant at $V_w = 0.5$ V when the probe was used with the CVA. On the other hand, the wire overheat was maintained constant at $a_w = 0.8$ when the probe was used with the CTA. The flow calibration curves obtained with both systems were already presented in Fig. 6.

A logarithmic wall-law plot of $u^+$ versus $y^+$, where $u^+ = \overline{U}/u_\tau$ and $y^+ = yu_\tau/\nu$ is presented in Fig. 10. There is about a decade of linear region, which is typical for a ZPG turbulent boundary layer at this Reynolds number (De Graaff and Eaton 2000). It is obvious from the figure that the results obtained with the CVA are comparable to those obtained with the CTA.

Profiles of the normalized streamwise stresses $\overline{u'^2}^+ = \overline{u'^2}/u_\tau^2$ are presented in Fig. 11. Here again, the data obtained with the CVA is fully consistent with that obtained with the CTA. The peak of $\overline{u'^2}^+$ observed in Fig. 11 is about 35 % lower than the value commonly accepted in the literature (De Graaff and Eaton 2000; Smits et al. 2011). This difference is caused by the spatial averaging of the signal which is dependent on sensor dimensions and independent of the type of anemometer. Ligrani and Bradshaw (1987) gave two criteria to ensure that the response of the wire is not attenuated in the region $y^+ < 200$: (1) the length to diameter ratio $l_w/d_w$ should be between 200 and 300 and (2) the length $l_w$ should be less than 20 times the viscous length scale $\nu/u_\tau$. In our case $l_w/d_w = 240$ and $l^+ = l_w/(\nu/u_\tau) = 78$. Given the large value of $l^+$, the attenuation in $\overline{u'^2}^+$ is not surprising.

The power spectral densities (PSD) of the fluctuating velocity at a position $y^+ = 114$ are presented in Figs. 12 and 13 on a log–log and a linear scale, respectively. The signals were acquired during 30 s with a sampling frequency of 204.8 kHz. The PSDs were calculated using Welch's modified periodogram method with 128 windows, 50 % overlap, and a Hamming window (Bendat and Piersol 2010). This resulted in a frequency resolution of 4.26 Hz. The effect of the software correction can clearly be observed in Fig. 12. The raw CVA curves (i.e., without software correction: green and pink lines) are lower than the CTA curve for $f > 200$ Hz. On the other hand, applying the software correction to the signals restores their energy (blue and red lines) so that all PSDs match well in the complete frequency range. Furthermore, Fig. 12 shows that the $T_{C_1}$ raw-signal (green line) is only slightly under-compensated, whereas the $T_{C_2}$ raw-signal (pink line) is largely under-compensated. This is consistent with the values of $M_{CVA} = 378$ µs (421 Hz), $T_{C_1} = 306$ µs (519 Hz),

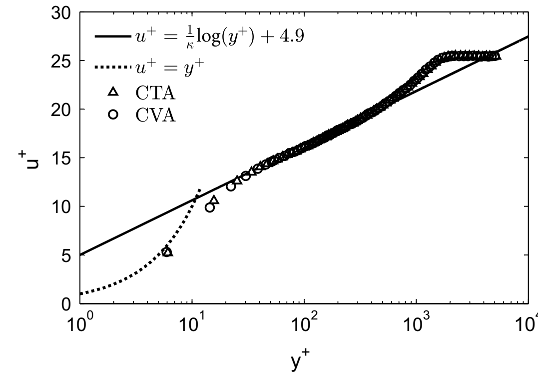


**Fig. 10** Logarithmic wall-law plot in ZPG boundary layer, $\kappa = 0.41$ Von Kármán constant

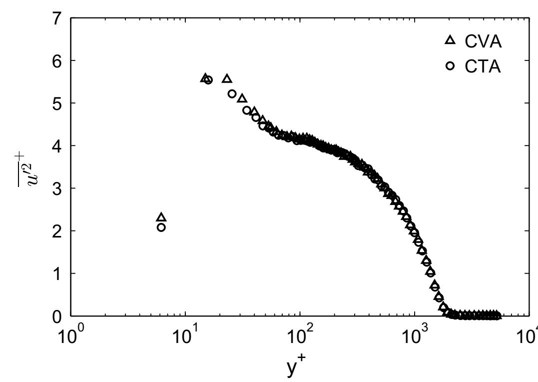


**Fig. 11** Profiles of normalized streamwise stresses in a ZPG boundary layer

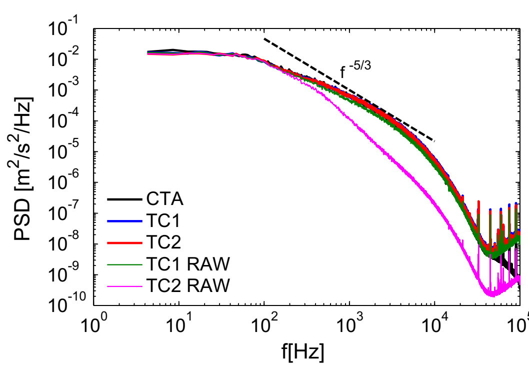


**Fig. 12** PSD of fluctuating velocity in a ZPG boundary layer at $y^+ = 114$ (log–log scale)

and $T_{C_2} = 73$ µs (2175 Hz). The PSDs obtained with both CVA-compensated and CTA are well superimposed in the complete frequency range, indicating that the CVA frequency compensation method (Eq. 8) is valid. The correspondence of the software-corrected CVA spectra with the

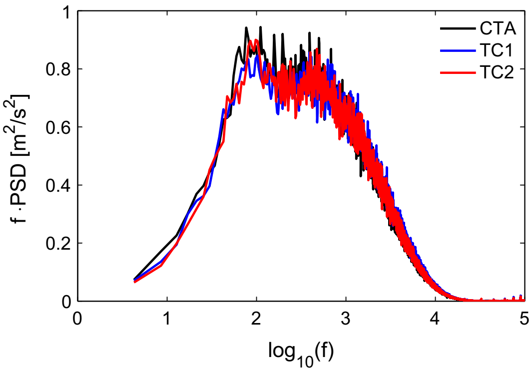


**Fig. 13** Premultiplied PSD of fluctuating velocity in a ZPG boundary layer at $y^+ = 114$ (linear scale)

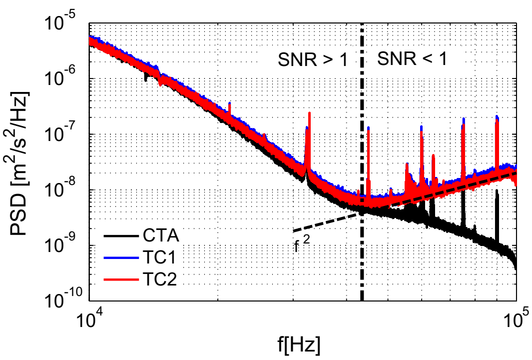


**Fig. 14** Magnified view of PSD at very high frequency ($y^+ = 114$). *SNR* signal-to-noise ratio

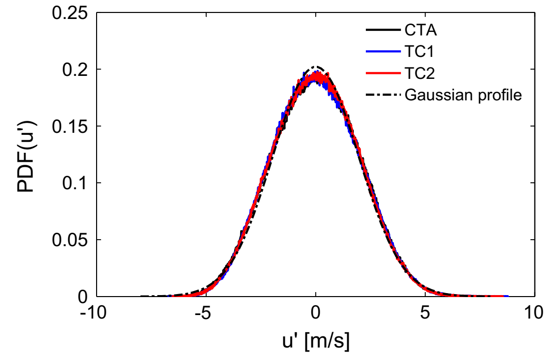


**Fig. 15** Probability density function of $u'$ at $y^+ = 114$

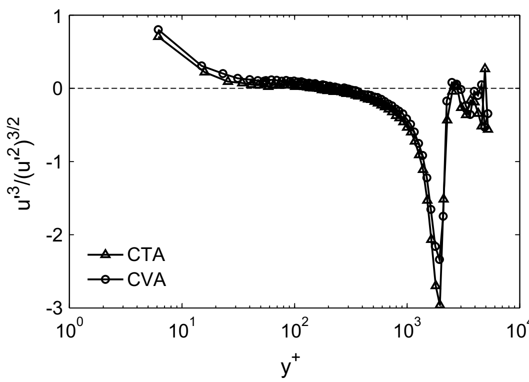


**Fig. 16** Profile of skewness factor $u'^3/(u'^2)^{3/2}$

CTA spectrum can also be clearly observed in the premultipied PSDs of Fig. 13.

Figure 14 shows a magnified view of the PSDs at very high frequencies. The CVA spectrum shows a typical $f^2$ rise, which is indicative of the electronic noise in the system (Weiss and Comte-Bellot 2004). This $f^2$ rise would also be observed in the CTA spectrum if its frequency roll-off occured at a higher value (Freymuth and Fingerson 1997). However, because of the frequency roll-off, only a small "kink" in the CTA PSD can be observed. Three conclusions can be reached from Fig. 14. First, the $f^2$ rise occurs almost exactly at the same frequency for both CVA and CTA ($f \simeq 43$ kHz), which indicates a similar level of signal-to-noise ratio (SNR) for both systems. At this position in the boundary layer ($y^+ = 114$), the signal is dominated by electronic noise for frequencies above 43 kHz, regardless of the type of anemometer. Second, the CTA bandwidth is just enough to reach the electronic noise limit in this flow configuration. The roll-off at $y^+ = 114$ appears to occur at a frequency lower than the 70 kHz measured in the free stream because of the reduced mean velocity. And finally, the CTA spectrum is slightly lower than the CVA spectrum above 20 kHz, whereas both spectra are perfectly superimposed at lower frequencies. This illustrates the difficulty in obtaining a perfectly flat frequency response with a CTA at frequencies close to its cutoff (e.g., Weiss et al. 2013; Hutchins et al. 2015).

Finally, Fig. 15 shows the probability density function (PDF) of the velocity fluctuations at $y^+ = 114$, and Fig. 16 shows the profile of the skewness factor $u'^3/(u'^2)^{3/2}$ across the boundary layer. Here also, the agreement between CVA and CTA is excellent. In Fig. 16 the large negative peak which appears at $y^+ \simeq 2000$ corresponds to the free edge of the boundary layer where intense bursts of negative $u'(t)$ are issued from the inner part of the boundary layer (Bailly and Comte-Bellot 2015).

### 4.2 Turbulent jet

Further comparative measurements between CVA and CTA were performed in a turbulent jet facility at Polytechnique Montréal (Sadeghi 2014). The nominal velocity at the nozzle exit (diameter $D = 3.4$ cm) was $U_{\mathrm{ref}} = 20$ m/s. Mean velocity and longitudinal velocity fluctuations were measured in the self-similar region of the jet at $x/D = 12$ with a

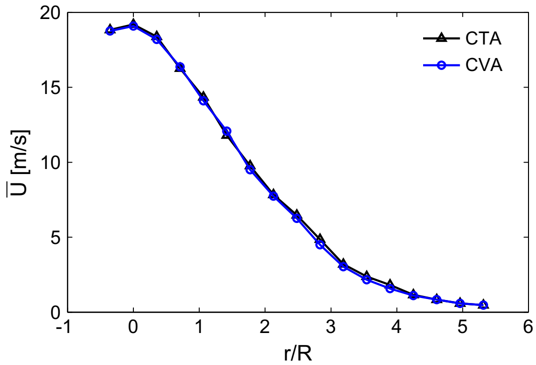


Fig. 17 Mean velocity profile at $x/D = 12$ in a round jet

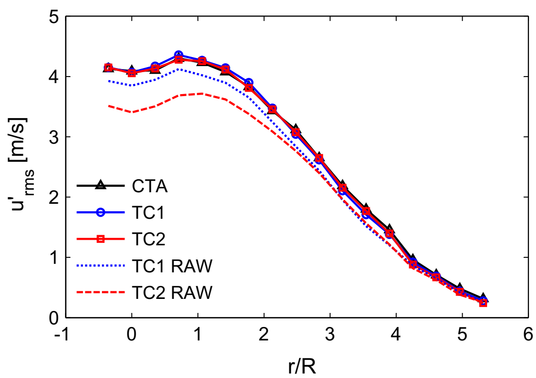


Fig. 18 RMS of fluctuating velocity in a round jet ($x/D = 12$)

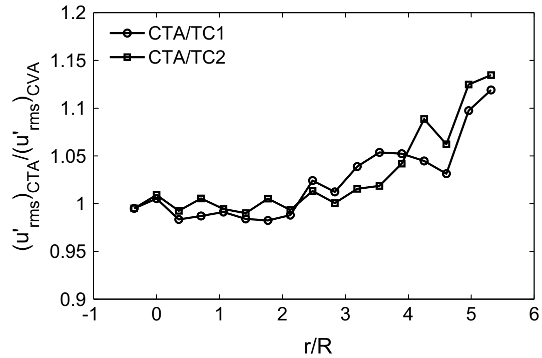


Fig. 19 Ratio of $u'_{\mathrm{rms}}$ measured with CTA and CVA

DANTEC 55P11 single-normal probe. No effort was spent to accurately characterize the flow structure since only a comparison between CVA and CTA operation of the hot-wire was of interest.

Figures 17 and 18 show radial profiles of the mean, respectively RMS, longitudinal velocity. The values obtained with the CVA and the CTA compare very well in both figures. The effect of the software correction (Eq. 8) on the RMS is illustrated in Fig. 18. Without software correction, the RMS of the uncompensated CVA signal is lower than that of the CTA signal. The difference is larger for the lower ($T_{C_2}$) value of the hardware compensation setting. This is expected since a lower value of the hardware compensation setting implies a wider uncompensated bandwidth between the hot-wire's (low-pass) cutoff and the amplifier's (high-pass) cutoff. As a reminder, in this configuration $M_{\mathrm{CVA}} = 394\,\mu\mathrm{s}$ (403 Hz), $T_{C_1} = 306\,\mu\mathrm{s}$ (519 Hz), and $T_{C_2} = 73\,\mu\mathrm{s}$ (2175 Hz).

Figure 19 gives further insight into the comparison of the fluctuating longitudinal velocity measured with both anemometers by showing the ratio of $u'_{\mathrm{rms}}$ measured with CTA and CVA. The ratio is essentially equal to one up to $r/R \simeq 3$, above which the CTA results become slightly larger than the CVA results. This small mismatch at large $r$ / $R$ is most likely caused by nonlinear effects linked to the very large turbulence level at these large distances from the jet centerline. Technically, a full nonlinear treatment like the one proposed by Berson et al. (2009) would be required to correct the CVA measurements. On the other hand, as demonstrated by Hussein et al. (1994), it is doubtful that a stationary hot-wire will provide reasonable results at such large $r$ / $R$ anyway, because of cross-flow and rectification errors. Therefore, no further effort was spent investigating this behavior.

Finally, Figs. 20 and 21 show a comparison of the pre-multiplied spectra at $r/R = 1$ and $r/R = 3$, respectively. For $r/R = 1$ the fluctuation level is about $u'_{\mathrm{rms}}/\overline{U} = 30\,\%$ and for $r/R = 3$ it is about $u'_{\mathrm{rms}}/\overline{U} = 55\,\%$. Despite these large turbulence levels, it is obvious that the agreement between CTA and CVA is excellent.

### 4.3 Practical considerations

The results presented in Sects. 4.1 and 4.2 have shown a very good agreement between the CVA and the more common CTA, which is currently the reference for practitioners of thermal anemometry. To complete the comparison, we now discuss the difference in effort required to obtain the turbulence data and in the uncertainty of the results.

The velocity calibration is essentially the same for both systems but the procedure used to ensure a flat frequency response is different. A CVA user has to perform a frequency compensation for each value of the mean flow velocity, whereas a CTA-user has to ensure that the cutoff frequency is high enough for the speed range of interest. In the case of the CVA, this implies that $T_{\mathrm{C}}$ and $M_{\mathrm{CVA}}$ must be experimentally determined, while in the case of a CTA, this implies that the circuit is properly tuned at the highest flow velocity to ensure circuit stability as the flow speed is varied. While the measurement of $T_{\mathrm{C}}$ is done only once (it is a constant in the CVA circuit), $M_{\mathrm{CVA}}$ needs to be determined

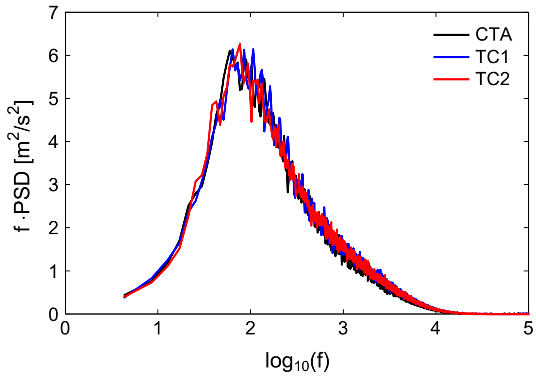


**Fig. 20** Premultiplied PSD of fluctuating velocity at $x/D = 12$ and $r/R = 1$ (linear scale)

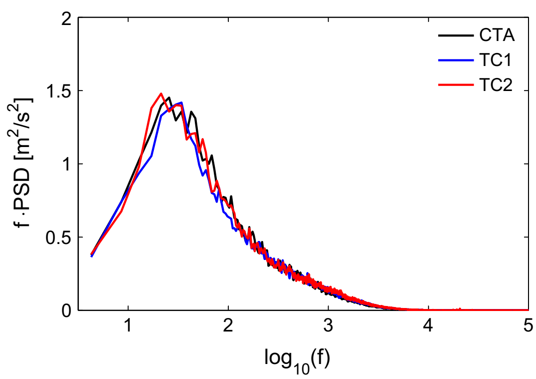


**Fig. 21** Premultiplied PSD of fluctuating velocity at $x/D = 12$ and $r/R = 3$ (linear scale)

at the start of a measurement campaign since it depends on sensor and flow conditions. We recommend to obtain $M_{\mathrm{CVA}}$ in parallel with the velocity calibration of the flow (e.g., Fig. 8). Thus, the production of the required data can be seen as an additional effort compared to CTA usage. On the other hand, the procedure can easily be automated and is not especially time consuming.

When a CTA is used to measure flow fluctuations at frequencies relatively close to its cutoff, the feedback circuit has to be carefully tuned at each mean velocity to ensure a flat frequency response at all conditions. This is because the transfer function of a CTA depends on the flow conditions, which means that only tuning the circuit at the highest mean velocity might produce an unsatisfactory frequency response as the velocity is diminished. A frequent tuning of the CTA circuit is at least as time consuming as the measurement of $M_{\mathrm{CVA}}$. Therefore, when velocity fluctuations with high frequency content are measured, we believe that the use of a CVA versus a CTA does not imply any additional effort. It is also worth mentioning that in some cases a perfect tuning of the CTA cannot be obtained with the available circuit parameters, which limits the frequency response of the system. For example, Hutchins et al. (2015) recently suggested that the frequency response of under- or over-damped CTA systems can only be considered approximately flat up to 5–7 kHz. Also, contrary to the CTA, the dynamic behavior of the CVA does not depend on the length of the hot-wire cable.

We now turn our attention to the difference in the uncertainty of the results for CVA and CTA. Again, the velocity calibration procedure for both systems is essentially the same. This means that the uncertainties in mean velocity are similar for CVA and CTA and depend on the uncertainties of the data acquisition procedure, the velocity reference, and possible hot-wire drift. In terms of velocity fluctuations, however, the two systems work differently. In a CTA the velocity fluctuation is directly obtained from the measured fluctuating output voltage that is processed by the calibration curve. In a CVA the velocity fluctuation is obtained from the corrected fluctuating voltage $v_s'^*(t)$, which itself depends on the measured output voltage $v_s'(t)$ and on both $T_{\mathrm{C}}$ and $M_{\mathrm{CVA}}$ (see Eq. 8). The uncertainties in $T_{\mathrm{C}}$ and $M_{\mathrm{CVA}}$ therefore represent an additional uncertainty component compared to the CTA (assuming, again, that the CTA is perfectly tuned, which is not necessarily the case).

A conservative estimate of the influence of uncertainties $\Delta T_{\mathrm{C}}$ and $\Delta M_{\mathrm{CVA}}$ in $T_{\mathrm{C}}$ and $M_{\mathrm{CVA}}$ can be obtained by considering Eq. 8 in the limit of high frequencies. For $f \gg 1/2\pi M_{\mathrm{CVA}}$ and $f \gg 1/2\pi T_{\mathrm{C}}$, we have $v_s'^*(t) \simeq (M_{\mathrm{CVA}}/T_{\mathrm{C}}) v_s'(t)$. The uncertainty $\Delta v_s'^*(t)$ in the corrected output voltage is therefore:

$$\left(\frac{\Delta v_s'^*}{v_s'^*}\right)^2 = \left(\frac{\Delta v_s'}{v_s'}\right)^2 + \left(\frac{\Delta M_{\mathrm{CVA}}}{M_{\mathrm{CVA}}}\right)^2 + \left(\frac{\Delta T_{\mathrm{C}}}{T_{\mathrm{C}}}\right)^2 \qquad (18)$$

Thus, the relative uncertainty in $v_s'^*$ is simply the root-sum-square of the relative uncertainties in the measured output voltage $v_s'$ and in the time constants $T_{\mathrm{C}}$ and $M_{\mathrm{CVA}}$. Based on the repeatability studies described in Sect. 3, we estimate $\Delta T_{\mathrm{C}}/T_{\mathrm{C}} \simeq \pm 1\ \%$ and $\Delta M_{\mathrm{CVA}}/M_{\mathrm{CVA}} \simeq \pm 2.6\ \%$ at the 95 % confidence level. This means that the CVA introduces a total additional uncertainty of less than $\pm 3\ \%$ in the fluctuating output voltage. This uncertainty then propagates into the value of the fluctuating velocity $u'(t)$. It should be noted, however, that this value is a conservative estimate that will only be realistic when most of the signal's energy is present at high frequency (i.e., for frequencies above $1/2\pi M_{\mathrm{CVA}}$ and $1/2\pi T_{\mathrm{C}}$). For the data presented in Figs. 13 and 20, most of the energy is actually observed at frequencies lower than $1/2\pi M_{\mathrm{CVA}}$. Processing this particular turbulence data with values of $T_{\mathrm{C}}$ and $M_{\mathrm{CVA}}$ selected so that $\Delta T_C/T_C = \pm 1\,\%$ and $\Delta M_{CVA}/M_{CVA} = \pm 2.6\,\%$, we obtain a $\Delta u'_{rms}/u'_{rms}$ of the order of ±1.5 %.

## 5 Conclusion

The method described in this article permits accurate measurements of turbulent fluctuations using a CVA. The method consists in three steps: (1) the calibration of internal elements, required to fit the actual circuit electronics to a simplified model involving only two electrical parameters; (2) a flow calibration to relate the average CVA output and the hot-wire time constant to average flow parameters; and (3) a specific data-processing algorithm to compute the fluctuating flow properties from the measured fluctuating output voltage. The method was validated by comparing its results with those of a research-grade CTA in two separate low-speed turbulent flows. In both flows (a turbulent boundary layer and a turbulent jet), the CVA results were shown to be essentially indistinguishable from the CTA results.

In terms of experimental procedure, the main difference between CVA and CTA is the necessity to accurately measure the hot-wire time constant $M_{CVA}$ when using a CVA. In contrast, the frequency compensation is automatic in the CTA, provided that the circuit is properly tuned using a square-wave test and that the achieved bandwidth is sufficient. The pros and cons of both systems in terms of effort required and uncertainties were discussed. In the authors' opinion, the principal advantages of the CVA compared to current CTA systems are its stability, its higher bandwidth, its well-behaved frequency response at high frequencies, and its limited sensitivity to cable length. We hope that our proposed procedure will help other researchers use CVA units in either low-speed or high-speed flows.

**Acknowledgments** The authors are grateful to Arun and Siva Mangalam from Tao Systems Inc. for providing a CVA unit and for their technical support. Part of this project was financed by the Samuel-De Champlain program established between the *ministère des Relations internationales du Québec* and the *ministère des Affaires étrangères et européennes de la République française*, 63rd session of the *Commission permanente de coopération franco-québécoise*.

## References

Bailly C, Comte-Bellot G (2015) Turbulence. Springer, Berlin

Bendat JS, Piersol AG (2010) Random data: analysis and measurement procedures, 3rd edn. Wiley, New York

Berson A, Blanc-Benon P, Comte-Bellot G (2009) A strategy to eliminate all nonlinear effects in constant-voltage hot-wire anemometry. Rev Sci Instrum 80(4):045102

Berson A, Poignand G, Blanc-Benon P, Comte-Bellot G (2010) Capture of instantaneous temperature in oscillating flows: use of constant-voltage anemometry to correct the thermal lag of cold wires operated by constant-current anemometry. Rev Sci Instrum 81(1):015102

Bruun HH (1995) Hot-wire anemometry: principles and signal analysis. Oxford University Press, Oxford

Collis D, Williams M (1959) Two-dimensional convection from heated wires at low reynolds numbers. J Fluid Mech 6(03):357–384

Comte-Bellot G (2007) Thermal anemometry. In: Tropea C, Yarin AL, Foss JF (eds) Handbook of experimental fluid mechanics. Springer, Berlin, pp 229–283

Comte-Bellot G, Sarma GR, Faure T, Dussauge JP, Dupont P, Debiève JF (1999) Performance studies of the constant voltage anemometer in a Mach 2.3 boundary layer. In: 18th international congress on instrumentation in aerospace and simulation facilities, Toulouse, France, vol paper 40

Comte-Bellot G, Weiss J, Béra JC (2004) Lead-resistance effects in a constant voltage anemometer. Rev Sci Instrum 75(6):2075–2081

De Graaff DB, Eaton JK (2000) Reynolds-number scaling of the flat-plate turbulent boundary layer. J Fluid Mech 422:319–346

Freymuth P, Fingerson LM (1997) Hot-wire anemometry at very high frequencies: effect of electronic noise. Meas Sci Technol 8(2):115–116

Horowitz P, Hill W (1989) The art of electronics, vol 2. Cambridge University Press, Cambridge

Hussein HJ, Capp SP, George WK (1994) Velocity measurements in a high-reynolds-number, momentum-conserving, axisymmetric, turbulent jet. J Fluid Mech 258:31–75

Hutchins N, Monty J, Hultmark M, Smits A (2015) A direct measure of the frequency response of hot-wire anemometers: temporal resolution issues in wall-bounded turbulence. Exp Fluids 56(1):1–18

Kegerise MA, Spina EF (2000a) A comparative study of constant-voltage and constant-temperature hot-wire anemometers Part I: the static response. Exp Fluids 29(2):154–164

Kegerise MA, Spina EF (2000b) A comparative study of constant-voltage and constant-temperature hot-wire anemometers: Part II: the dynamic response. Exp Fluids 29(2):165–177

Ligrani PM, Bradshaw P (1987) Subminiature hot-wire sensors: development and use. J Phys E Sci Instrum 20(3):323–332

Mangalam S, Sarma G, Kuppa S, Kubendran L (1992) A new approach to high-speed flow measurements using constant voltage anemometry. In: AIAA 92-3957, 17th Aerospace ground testing conference

Mohammed-Taifour A, Schwaab Q, Pioton J, Weiss J (2015) A new wind tunnel for the study of pressure-induced separating and reattaching flows. Aeronaut J 119(1211):91–108

Perry AE (1982) Hot-wire anemometry. Oxford University Press, Oxford

Sadeghi A (2014) Investigation of the frequency response of constant voltage anemometers in turbulent flows. Master's thesis, École Polytechnique de Montréal

Sarma G, Comte-Bellot G, Faure TM (1998) Software corrected hot wire thermal lag for the constant voltage anemometer featuring a constant bandwidth at the selected compensation setting. Rev Sci Instrum 69(9):3223–3231

Sarma GR (1998) Transfer function analysis of the constant voltage anemometer. Rev Sci Instrum 69(6):2385–2391

Sarma GR, Comte-Bellot G (2002) Automated constant voltage anemometer for measurements with fluid temperature drifts. Rev Sci Instrum 73(3):1313–1317

Sarma GR, Lankes RW (1999) Automated constant voltage anemometer with in situ measurements of overheat and time constant of the hot wire. Rev Sci Instrum 70(5):2384–2386

Smits AJ, McKeon BJ, Marusic I (2011) High-reynolds number wall turbulence. Annu Rev Fluid Mech 43:353–375

Truzzi GE, Sarma GR, Chokani N (2002) Constant voltage anemometer operated hot wire at subsonic speeds over wide overheats in unsteady flows. Rev Sci Instrum 73(12):4363–4368

Weiss J (2003) Effect of bridge imbalance on the estimation of sensitivity coefficients for constant-temperature hot-wire anemometers. Meas Sci Technol 14(8):1373–1380

Weiss J, Comte-Bellot G (2004) Electronic noise in a constant voltage anemometer. Rev Sci Instrum 75(5):1290–1296

Weiss J, Knauss H, Wagner S (2001) Method for the determination of frequency response and signal to noise ratio for constant-temperature hot-wire anemometers. Rev Sci Instrum 72(3):1904–1909

Weiss J, Chokani N, Comte-Bellot G (2005) Constant-temperature and constant-voltage anemometer use in a mach 2.5 flow. AIAA J 43(5):1140–1143

Weiss J, Berson A, Comte-Bellot G (2013) Investigation of nonlinear effects in constant-temperature anemometers. Meas Sci Technol 24(8):085,302